SPECIAL MERRA COLLECTION

Global Energy and Water Budgets in MERRA

MICHAEL G. BOSILOVICH

NASA GSFC GMAO, Greenbelt, Maryland

FRANKLIN R. ROBERTSON

NASA MSFC, Huntsville, Alabama

JUNYE CHEN

ESSIC, University of Maryland, College Park, College Park, and NASA GSFC GMAO, Greenbelt, Maryland

(Manuscript received 28 October 2010, in final form 10 March 2011)

ABSTRACT

Reanalyses, retrospectively analyzing observations over climatological time scales, represent a merger between satellite observations and models to provide globally continuous data and have improved over several generations. Balancing the earth's global water and energy budgets has been a focus of research for more than two decades. Models tend to their own climate while remotely sensed observations have had varying degrees of uncertainty. This study evaluates the latest NASA reanalysis, the Modern Era Retrospective-Analysis for Research and Applications (MERRA), from a global water and energy cycles perspective, to place it in context of previous work and demonstrate the strengths and weaknesses.

MERRA was configured to provide complete budgets in its output diagnostics, including the incremental analysis update (IAU), the term that represents the observations influence on the analyzed states, alongside the physical flux terms. Precipitation in reanalyses is typically sensitive to the observational analysis. For MERRA, the global mean precipitation bias and spatial variability are more comparable to merged satellite observations [the Global Precipitation and Climatology Project (GPCP) and Climate Prediction Center Merged Analysis of Precipitation (CMAP)] than previous generations of reanalyses. MERRA ocean evaporation also has a much lower value, which is comparable to independently derived estimate datasets. The global energy budget shows that MERRA cloud effects may be generally weak, leading to excess shortwave radiation reaching the ocean surface.

Evaluating the MERRA time series of budget terms, a significant change occurs that does not appear to be represented in observations. In 1999, the global analysis increments of water vapor changes sign from negative to positive and primarily lead to more oceanic precipitation. This change is coincident with the beginning of Advanced Microwave Sounding Unit (AMSU) radiance assimilation. Previous and current reanalyses all exhibit some sensitivity to perturbations in the observation record, and this remains a significant research topic for reanalysis development. The effect of the changing observing system is evaluated for MERRA water and energy budget terms.

1. Introduction

In the study of the earth's climate, quantifying global water and energy cycling rates and the associated physical processes more accurately is critical to understanding the climate and its mechanisms of variability and change from global to local scales. The sun heats the atmosphere and the surface, thus driving many processes including the transfer of energy and water and ultimately dynamical transports of these quantities. Trenberth et al. (2009, hereafter TFK09) provide discussion on the primary water and energy transfer processes, as well as recent quantitative assessments of various observational data and uncertainties. Even though the top of the atmosphere

Corresponding author address: Michael G. Bosilovich, Global Modeling and Assimilation Office, Code 610.1, NASA Goddard Space Flight Center, Greenbelt, MD 20771.
E-mail: michael.bosilovich@nasa.gov

DOI: 10.1175/2011JCLI4175.1

(TOA) radiative fluxes likely have the smallest uncertainties (order 5 W m^{-2} bias and, perhaps, an order of magnitude smaller in precision), refining this observational record is still an active area of research (Loeb et al. 2009). Validating the observed water cycle observations through global balance shows that the uncertainties are a fundamental issue (Schlosser and Houser 2007). While some observational uncertainty is steadily narrowing, few of the processes have adequate observational representation. In this case, modeled estimates of the energetics derived from retrospective analyses (or reanalyses) have been used to fill gaps in the data. But of course, models themselves, which represent our understanding of the earth's processes, are limited by computational resources and simplifying assumptions. Models have their own uncertainty and can evolve their own climate, leading to distinct bias when compared with available observations. Data assimilation can produce analyses of the observed state that constrains the model's physical results. Reanalyses apply data assimilation across climate time scales in an effort to provide globally continuous and consistent climate data that exploit both observations and models. However, individual reanalyses still must contend with uncertainty, for example, different reanalyses respond to global forcing with different circulation perturbations (Chen et al. 2008a). With several generations of reanalyses to consider, the various datasets generated from these efforts show large variance in the processes of the global water and energy budgets (Chen et al. 2008a,b; TFK09; Bosilovich et al. 2008, 2009).

Kalnay et al. (1996), Uppala et al. (2005), and Onogi et al. (2007) provide some of the most important overviews of existing long global reanalyses. In this study, we evaluate the global energy and water cycles of a new reanalysis, the NASA Modern Era Retrospective-Analysis for Research and Applications (MERRA) (Rienecker et al. 2011). MERRA data are derived from the Goddard Earth Observing System version 5 (GEOS-5) data assimilation system, which is a combination of a NASA general circulation model (Rienecker et al. 2007) and the gridpoint statistical interpolation (GSI) analysis developed in collaboration with the National Centers for Environmental Prediction. During the validation of GEOS-5 and preparations for MERRA, special attention was given to the water and energy cycles; however, the validation experiments themselves were limited in time (e.g., Bosilovich et al. 2008). Given the established biases in space and time of the water and energy cycles in existing reanalyses, MERRA water and energy cycles need to be diagnostically characterized in comparison with the available observations and reanalyses.

2. Data

a. Reanalyses

There exist several atmospheric reanalyses for the period of 1979 through current time. The Japanese 25-yr Reanalysis (JRA-25), released for use in March 2006 (Onogi et al. 2005, 2007); the 40-yr European Centre for Medium-Range Weather Forecasts Re-Analysis (ERA-40; Uppala et al. 2005), which stops in August 2002; and the National Centers for Atmospheric Research–Department of Energy second reanalysis (NCEP–DOE R2; Kanamitsu et al. 2002) represent the second generation of reanalyses. More recently, ECMWF has also released a short period (1989–present) interim (ERA-Interim) reanalysis with their latest data assimilation system (Simmons et al. 2007; Uppala et al. 2008). The NCEP Climate Forecast System Reanalysis (CFSR) (Saha et al. 2010) became available in early 2010. While all of these reanalyses assimilate observations over the recent climate record, new reanalyses will continue to be produced because of updated model physical processes, enhanced data assimilation methods, increased availability of computing resource, growing types of observations available for assimilation, and improved observational quality control.

While the data assimilation and numerical model components of the reanalysis system are fixed for the processing of the climate period (as proposed by Bengtsson and Shukla 1988; Trenberth and Olson 1988), the observing system changes greatly in time. A major change to the observational record concerns the onset of routine operational remote sensing soundings, starting with *TIROS-N* followed by *NOAA-6* in 1979, before which primarily conventional (e.g., radiosonde and surface stations) were available. Bengtsson et al. (2004) studied the full 40-yr time series of ERA-40 and found that unrealistic trends occurred related to increased satellite observations in 1979. However, even during the modern satellite observing period, new satellites and measurements start and end at irregular intervals, and ultimately, any given satellite has an expected lifetime on the order of 10 years, much shorter than what is needed for climate studies. So, there are numerous changes to the remotely sensed data record (Rienecker et al. 2011) that involve not only calibration (bias) but also measurement sensitivity and sampling density. These variations during the satellite era can lead to systematic changes in the reanalysis time series. For example, the JRA-25 precipitation record is sensitive to the availability of microwave total column water retrievals (Onogi et al. 2005; Bosilovich et al. 2008) beginning in 1987 with the Special Sensor Microwave Imager (SSM/I) operational satellites.

While analysis state variables are most closely related to observations, the variability of the physical processes

and fluxes among reanalyses can be substantial (Bosilovich et al. 2009). Much of the reanalysis data that provide information about the earth's water and energy budgets come from the model physics, which has been categorized as being closely related to the numerical model as opposed to the analyzed state fields (Kalnay et al. 1996). Despite the shortcomings, a particular advantage of reanalyses in climate studies is the availability of all or many of the earth's energy and water budget component fluxes. For example, NCEP reanalyses have played a significant role in the development of global merged observational precipitation [Climate Prediction Center Merged Analysis of Precipitation (CMAP)] (Xie and Arkin (1996); and ocean evaporation Yu and Weller (2007)]. Ultimately, activities such as hydrologic applications would like to make use of reanalyses, but the accuracy of model physics that control the fluxes requires further development (e.g., Maurer et al. 2001). The physical terms of the reanalysis budgets generally do not balance even over long periods because the atmospheric data assimilation provides additional constraint (or forcing) in the balance of the output data. This is ultimately presented as a residual term in many studies (Roads and Betts 2000; Roads et al. 2002). This term, referred to here as the analysis increment, reflects the observations effect on the analysis, and, as the observations change so do the forcing and the physical response of the model to the forcing. With this term quantified, the budgets can be studied closely, and some work has used the information to apply corrections to the physical terms (Schubert and Chang 1996; Bosilovich and Schubert 2001; Robertson et al. 2011).

In reviewing the observed global energy budget, TFK09 also compared the reanalysis energy budgets (specifically ERA-40, NCEP–DOE R2, and JRA-25), and some similar biases are evident. First, the net TOA energy did not balance well, with too much upward flux. However, JRA-25 bias is related to too much outgoing longwave radiation (OLR), while NCEP–DOE R2 is due to too much reflected shortwave radiation, but both imbalances were on the order of 10 W m^{-2}. Also, all reanalyses had excessive evaporation and precipitation leading to stronger global hydrologic cycling. One aspect of the reanalyses budgets not addressed by TFK09 is the atmospheric imbalance related to the analysis increment. The observations can act as a source or sink of water and energy, and in their study, the assimilated observational analysis generally add energy to the system though it is dissipated in different ways.

b. MERRA

MERRA is a reanalysis of the satellite era (1979–present) using the GEOS-5 data assimilation system. Rienecker et al. (2007) thoroughly describe the MERRA/GEOS-5 numerical model and data assimilation system, while Rienecker et al. (2011) describe the MERRA project. In addition to the conventional observations (radiosonde, station, aircraft, ship), SSM/I radiances, TIROS Operational Vertical Sounder (TOVS) radiances, Atmospheric Infrared Sounder (AIRS) radiances, and scatterometer wind retrievals (to name a few) are also assimilated. MERRA was run in three separate data streams, each of which were initialized with spun up states from a long climate model simulation, then two years of coarse-resolution data assimilation followed by at least four years of data assimilation for the last two data streams (i.e., using the actual observations at the native horizontal resolution, not spinning the same year over again) at the MERRA native grid (Rienecker et al. 2011 describes the spinup experiments). The native MERRA grid has a spatial resolution of ½° latitude by ⅔° longitude with 72 hybrid model levels in the vertical (Suarez et al. 2011). The analysis is performed by the NCEP GSI (Wu et al. 2002). The model is then updated with an additional model segment that includes an incremental analysis update (IAU) in the budget equations (Bloom et al. 1996). The shock of the analysis at the forecast initialization is greatly reduced so that the spindown of physical fields (e.g., precipitation) is a small factor in this system. This is also where observations affect the model's governing equations (discussed in the next section). Bosilovich et al. (2008) evaluate precipitation from the GEOS-5 data assimilation validation experiments for the months of January and July 2004 and compare with the existing reanalyses and merged satellite observations of precipitation GPCP and CMAP to assess the character of the monthly precipitation prior to the production of MERRA. The results were promising but limited due to the short period of the validation experiments and will be briefly revisited later in this study.

c. Budget equations

MERRA output diagnostics encompass all the variables required to balance energy and mass budgets for the atmosphere and land. The MERRA enthalpy budget is produced, where we define enthalpy $H = \overline{c_p T_v}$ (c_p is the heat capacity of dry air at constant pressure, and T_v is the virtual temperature). The enthalpy budget is written

$$\frac{\partial H}{\partial t} = -\nabla \cdot \overline{(\mathbf{V} c_p T_v)} + \overline{\omega\alpha} + \left[\frac{\partial H}{\partial t}\right]_{\mathrm{RAD}} + \left[\frac{\partial H}{\partial t}\right]_{\mathrm{MST}} + \left[\frac{\partial H}{\partial t}\right]_{\mathrm{ANA}} + \left[\frac{\partial H}{\partial t}\right]_{\mathrm{TRB}} + \mathcal{R}. \quad (1)$$

Overbars denote a vertical integration over the mass of the atmosphere. The first two terms on the right-hand side of the equation represent the convergence and release of potential energy. The other tendencies represent radiation (RAD), moist processes (MST), and turbulent diffusion (TRB, in this example, the sensible heat flux). The analysis increment (ANA) is the tendency that is added to the prognostic budgets due to the observational analysis. Here $\mathcal{R}$ is a small value that in this case includes the conversions of energy to/from kinetic energy (in diffusion and mechanical generation), gravity wave drag, and a residual that results from maintaining energy balance in the presence of numerical dissipation, each of which are also included in the output diagnostics (Suarez et al. 2011). The vertically integrated radiation term can be expanded to its top of the atmosphere and surface boundary conditions:

$$\left[\frac{\partial H}{\partial t}\right]_{\mathrm{RAD}} = (\mathrm{SW}_T - \mathrm{SW}_S) - (\mathrm{OLR} + \mathrm{LW}_S). \tag{2}$$

The radiation term includes solar [net shortwave (SW), at the top of the atmosphere T and at the surface S] radiation, the net surface longwave radiation (LW_S), and the outgoing longwave radiation (OLR) at the top of the atmosphere. The MST term includes all the heating due to moist processes, including the condensation heating and evaporation in all phases, and here, the vertical integral of the MST term is the latent heat resulting from the production of precipitation.

The MERRA vertically integrated total water (w) budget for all phases can be written as

$$\frac{\partial w}{\partial t} = -\nabla \cdot \overline{(\mathbf{V}w)} + (E - P) + \left[\frac{\partial w}{\partial t}\right]_{\mathrm{ANA}} + F \tag{3}$$

$$w = \overline{q}_v + \overline{q}_l + \overline{q}_i. \tag{4}$$

The change of total water is related to the dynamical convergence of water and the physical processes of evaporation and precipitation (sum of convective, large-scale, and frozen forms). In the MERRA system, two nonphysical terms affect the moisture budget. Here F represents a very small amount of negative filling, ensuring positive water vapor content (less than 0.04% of precipitation or evaporation globally averaged). However, the ANA term represents the analysis increment of water vapor, which is on the order of magnitude of $E - P$. ANA is the water vapor forcing needed to constrain the evolution of the reanalysis steps to reconcile with all the various observations of water vapor, both explicit observations as well as the effects in satellite channel radiances sensitive to moisture. As the MERRA system cycles in time, it performs a forecast, analysis, and then assimilation segment. The assimilation segment is essentially a model forecast that includes the ANA or analysis increment tendencies discussed previously. These budgets, and most MERRA output diagnostics, are derived from the assimilation segment. A result of cycling the system in this way is that the observational analysis tendencies can be quantified alongside the physical model data. The result is that long-term globally averaged water balances, not just E and P but the analysis increment, must be accounted for as well. The analysis increment is the forcing applied to a cycle of the model simulation, developed from the analysis of observations and comparing the analysis to a forecast cycle (Bloom et al. 1996). Additional information on the formulation of the budgets is discussed by Rienecker et al. (2007) and Suarez et al. (2011).

3. Water and energy budgets

a. Global mean climatology

TFK09 collect the global energy budget data from various sources, observational and reanalyses, and close it with consistency arguments from dataset intercomparisons, to determine estimates for principal energy flux components and balance. However, each term exhibits large variations among the different observing systems and reanalyses, so any determination of the global average energy budget still includes significant uncertainty. The spatial and temporal variations then are much more difficult to know with certainty. We will characterize the MERRA global energy budget in terms of the existing data and analysis, to identify those aspects which are realistic at global scales, with some further analysis of regional scales.

Table 1 compares the results of the TFK09 evaluation of energy fluxes with MERRA values during the same March 2000 to May 2004 period (see TFK09 for the values from other reanalyses and observed data, their Table 2). At the top of the atmosphere the MERRA net radiative flux is slightly negative (-0.2 W m^{-2}), which compares favorably with an adjusted International Satellite Cloud Climatology Project (ISCCP) estimate of 0.9 W m^{-2} warming (TFK09). We note that the current unadjusted Clouds and the Earth's Radiant Energy System (CERES) TOA imbalance is in excess of 6 W m^{-2} (TFK09). The MERRA net flux is closer to the observed estimates than the JRA-25 and National Centers for Environmental Prediction–National Center for Atmospheric Research (NCEP–NCAR R1) reanalyses. Comparing the TOA components of the net radiation, MERRA OLR is

TABLE 1. Energy fluxes (March 2000–May 2004) partitioned by global, land, and ocean averages comparable to the estimates developed by TFK09 (their Table 2). TFK09 also provide ISSCP-FD, NCEP reanalyses, JRA-25, and WHOI and HOAPS ocean fluxes. The mean annual cycle is computed first, then the annual average is computed.

(a) TOA

	Solar transmitted	Solar reflected	Albedo (%)	Solar net	OLR	Net down
			Global			
MERRA	341.3	99.6	29.2	241.7	242.0	−0.2
TFK09	341.3	101.9	29.8	239.4	238.5	0.9
			Land			
MERRA	325.7	106.8	32.8	218.9	232.9	−14.0
TFK09	330.2	113.4	34.4	216.8	232.4	−15.6
			Ocean			
MERRA	347.9	96.6	27.8	251.2	245.7	5.5
TFK09	345.4	97.8	28.3	247.7	240.8	6.9

(b) Surface

	Solar absorbed	Solar net	Solar reflected	LH	SH	LW up	LW down	LW net	Net down
				Global					
MERRA	72.7	169.1	23.6	76.4	18.3	394.3	330.3	64.0	9.4
TFK09	78.2	161.2	23.1	80.0	17.0	396.0	333.0	63.0	1.2
				Land					
MERRA	68.7	150.2	46.7	44.9	33.2	364.6	294.6	70.0	2.0
TFK09	78.0	145.1	39.6	38.5	27.0	383.2	303.6	79.6	0.0
				Ocean					
MERRA	74.3	176.9	14.0	89.5	12.1	406.6	345.2	61.5	13.8
TFK09	78.2	167.8	16.6	97.2	12.0	400.8	343.2	57.6	1.3

larger than the TFK09 estimates (and also observations in their Fig. 2) while the reflected shortwave radiation is underestimated, suggesting the effect of clouds is weaker than expected. Similarly, at the surface, downward longwave radiation is underestimated while the surface downward shortwave radiation is overestimated.

Since MERRA and the reanalyses considered in TFK09 use prescribed SST, the ocean temperatures and heat content do not respond to the net downward flux at the ocean surface (e.g., 13.8 W m^{-2} in MERRA). While MERRA has a significant global average flux of heat from the atmosphere to the ocean, the JRA surface flux sign is reversed (TFK09, Table 2). The NCEP reanalysis shows little average net flux (TFK09, Table 2), especially over the oceans, but at the expense of unrealistic solar reflection. A significant component of this difference between MERRA and JRA is the ocean surface evaporation, for which MERRA is much lower than JRA. TFK09 (their Table 2) provide merged observation-based estimates from the Hamburg Ocean Atmosphere Parameters and Fluxes from Satellite Data (HOAPS) and Woods Hole Oceanographic Institution (WHOI) evaporation, but a large discrepancy exists between them. This emphasizes the significant remaining variations

TABLE 2. As in Table 1 but for the MERRA 30-yr base climate period 1979–2008. Units in W m^{-2}.

(a) TOA–30 year (1979–2008)

	Solar transmitted	Solar reflected	Albedo (%)	Solar net	OLR	Net down
Global	341.3	96.4	28.2	245.0	242.5	2.4
Land	325.7	106.5	32.7	219.2	231.9	−12.7
Ocean	347.9	92.2	26.5	255.7	247.0	8.7

(b) Surface–30 year (1979–2008)

	Solar absorbed	Solar net	Solar reflected	LH	SH	LW up	LW down	LW net	Net down
Global	72.1	172.9	24.0	75.1	18.1	393.3	327.8	65.5	13.3
Land	68.6	150.5	46.8	44.9	33.5	363.2	293.1	70.2	2.1
Ocean	73.5	182.2	14.4	87.7	11.6	405.9	342.2	63.6	19.3

TABLE 3. The land and ocean water and energy budgets including transport (dw/dtDYN and dH/dtDYN) between land/ocean from MERRA 30-yr average. The water budget terms are evaporation (E), precipitation (P), and water vapor analysis increment (dw/dtANA). The energy budget terms are net fluxes at the surface (SFC) and TOA, analysis increment of enthalpy (dH/dtANA) and heating of due to the analysis of water ($dH/dt\mathrm{ANA}_w$).

Water budget ($\times 10^3$ K m^3 yr^{-1})				
	E	P	dw/dtANA	dw/dtDYN
Land	87	116	−9	39
Ocean	405	368	1	−39

Energy budget (PW)					
	SFC	TOA	dH/dtANA	$dH/dt\mathrm{ANA}_w$	dH/dtDYN
Land	−0.1	−2.0	3.4	−0.7	−0.6
Ocean	−6.5	2.9	2.8	0.1	0.6

among reanalyses and recent satellite-based estimates. It is anticipated that the emerging Seaflux dataset (C. A. Clayson et al. 2011, personal communication) will narrow the uncertainties for observed data products. A similar conclusion can also be reached for land fluxes (Vinukollu et al. 2011) for which analyses fluxes are collectively biased and more variable than observervation-based products. Furthermore, the averaging period may affect the global averages. For reference, Table 2 shows MERRA data similar to Table 1, except for the 30-yr base period of 1979–2008. In some variables, differences of a couple W m^{-2} are evident. The 30-yr total net heating of the surface is 13.3 W m^{-2}, which is ~4 W m^{-2} greater than the TFK09 base period average. Temporal variations of the MERRA water and energy cycles are discussed in section 4.

Fasullo and Trenberth (2008a,b) and Trenberth et al. (2009) partition the water and energy budgets into land and ocean components to compute the transport from land to ocean. Table 3 provides this partitioning for the MERRA water and energy budgets and solving for the transport. A fundamental difference from the previously cited calculations is the presence of the analysis increments in the MERRA budgets. Considering that the increments represent a corrective tendency accounting for much of the mean error of the water state at any given time, the magnitude of these terms in the MERRA budgets is quite large and cannot be neglected.

For energy, the top of the atmosphere and land surface fluxes appear comparable to the Fasullo and Trenberth (2008a) estimates. The large downward surface flux over the ocean, mentioned previously, is quite apparent in the energy budget and is likely influencing the ocean–land energy transport (the sign of the flux is opposite to that computed by Fasullo and Trenberth 2008a). We noted earlier that the imbalance of energy in the JRA-25 ocean radiation is about the same magnitude as MERRA but opposite in sign, indicating that different reanalyses could manifest different water and energy transport characteristics. For the global water budget, the moisture transport value is generally comparable to that diagnosed by Trenberth et al. (2007, 2011), and the magnitudes of the increments are smaller than that of $P - E$. Trenberth et al. (2011) updates this evaluation with transport calculations from eight reanalyses including MERRA, showing the variability across them [30–40 ($\times 10^3$ K m^3 yr^{-1})]. While this seems reasonable for a long-term average, the temporal variations during the period also need to be considered (Section 4).

b. Spatial variations

As discussed in the previous section, biases in cloud radiative effects play a role in the MERRA representation of the surface energy budget. Figure 1 compares the TOA longwave cloud effect of MERRA and other reanalyses with that computed from the surface radiation budget (SRB) dataset (P. W. Stackhouse et al. 2011, personal communication). Positive values indicate that the MERRA cloud effect is weaker than for SRB in the global average, driven by the extratropical regions. In MERRA, the tropics have more cloud effect similar to the inter-America seas (IAS) region (this tends toward boreal summer, not shown). On the other hand, extratropical regions have a weaker cloud effect, generally during the boreal winter (not shown). The center of the ITCZ in the eastern tropical Pacific Ocean is also weaker in MERRA than SRB. The NCEP reanalyses show reasonable comparison to the SRB data except that the CFSR South Pacific convergence zone (SPCZ) has a notably weak bias. The ECMWF and JRA reanalyses have generally weaker cloud effect everywhere (with the exception of some increased cloud effect in ERA40 tropical oceans). In this global evaluation, high-latitude clouds and radiative effects are not apparent. Cullather and Bosilovich (2011a,b) examine the high-latitude regional water and energy budgets more closely.

A distinctive feature of the MERRA global comparisons in the previous section is the surface evaporation, especially over the ocean, when comparing with all the data reported in TFK09 (Table 1). While most reanalyses show higher oceanic evaporation than WHOI objectively analyzed air–sea fluxes (OAFlux) on a global basis, MERRA is lower. Figure 2 shows ocean-only difference fields of surface evaporation with the OAFlux dataset (Yu and Weller 2007). The systematic MERRA low bias in the extratropics apparent over the warm western boundary current regions distinguishes it from other reanalyses. This behavior has been attributed by Roberts

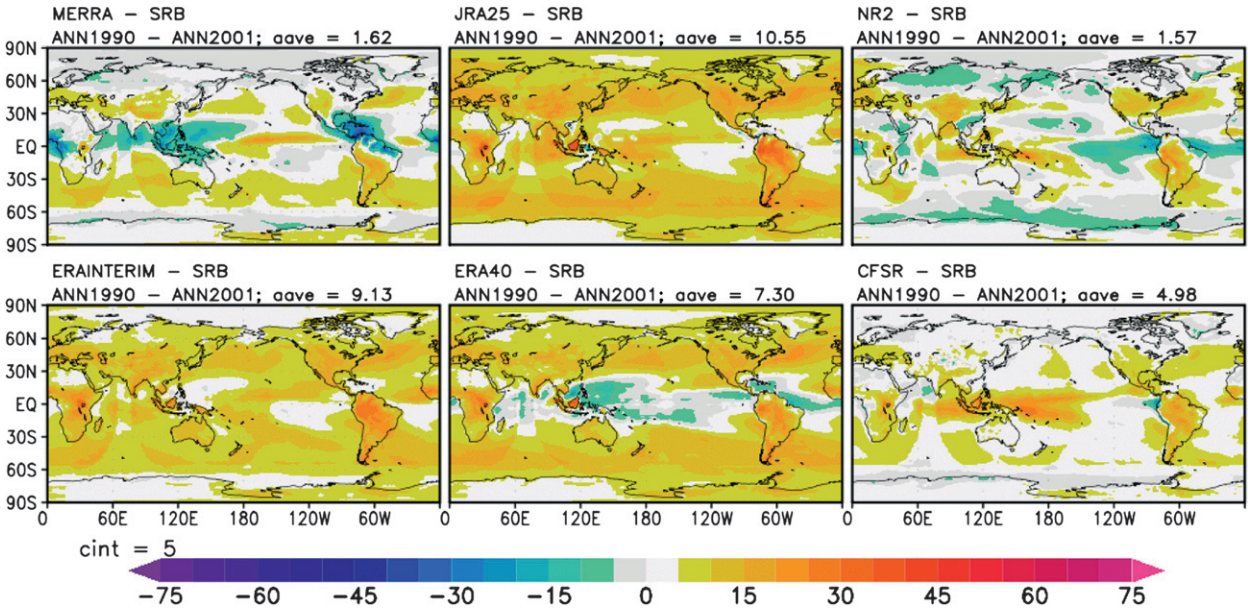

FIG. 1. Annual differences (1990 − 2001) of MERRA and other reanalyses longwave cloud effect from that of the surface radiation budget (SRB) data. Here, the longwave effect is the TOA all-sky minus the clear-sky outgoing longwave radiation, such that positive difference indicates the reanalysis cloud effect is less than SRB. The global area average of each map is included in the upper right corner of each panel. Additional figures are available from The MERRA Atlas (GMAO 2011).

et al. (2011) to smaller vertical surface moisture gradients ($q_s - q_a$). They provide evidence that $q_s - q_a$ underestimates are particularly strong during strong cold air outbreaks. In contrast, within tropical regions MERRA biases relative to OAFlux are at least as small as those of other reanalyses with systematically large biases over high SST gradient regions, particularly in the subtropical eastern South Pacific.

Figure 3 shows the seasonal precipitation comparison among MERRA and other reanalyses with GPCP (version 2.0 Adler et al. 2003) merged precipitation data. For MERRA, the tropics precipitation tends to be

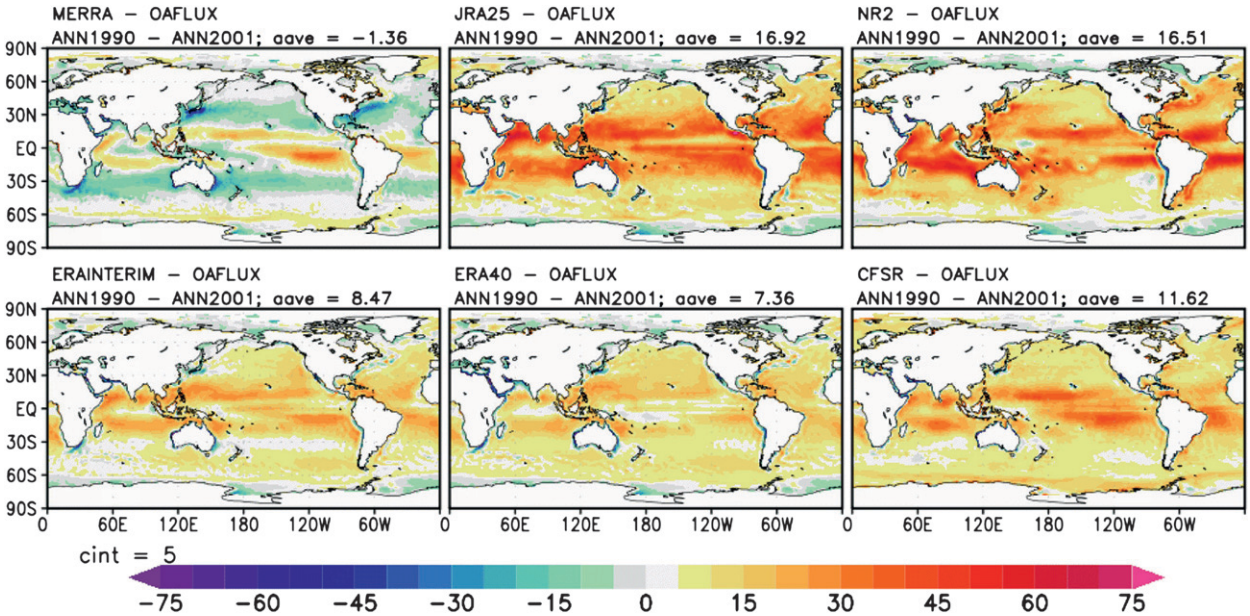

FIG. 2. Annual differences (1990 − 2001) between MERRA and other reanalyses ocean surface latent heat flux and that of OAFlux merged data (Yu and Weller 2007). Positive flux is directed upward.

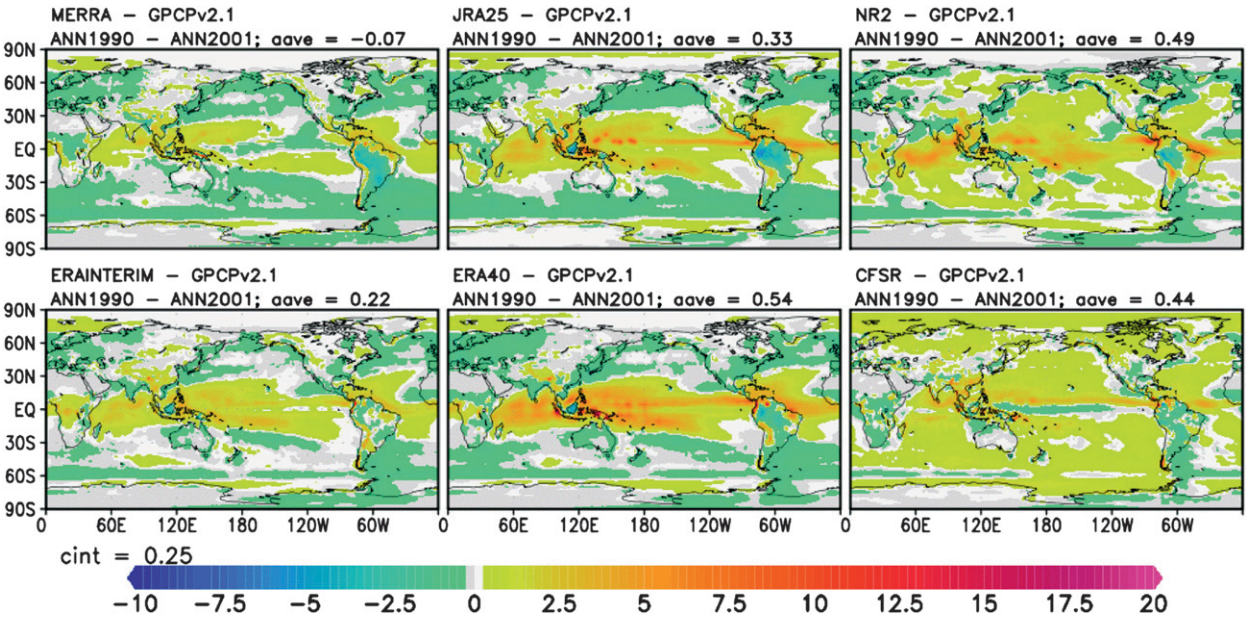

FIG. 3. Annual differences (1990 − 2001) between MERRA and other reanalyses precipitation with GPCP merged data (Adler et al. 2003).

overestimated with the midlatitudes underestimated, which is typical among reanalyses. The MERRA tropical bias, though, is less than the other reanalyses. Many of the precipitation biases apparent here are also consistent with the biases noted in comparing MERRA and TOA longwave cloud effect (Fig. 1). For example, in the IAS and tropical western Pacific regions where the MERRA cloud effect exceeds SRB, the precipitation is overestimated. Likewise, in the southern midlatitudes MERRA precipitation is slightly underestimated where the cloud effect is weaker. Reanalyses have been shown to be internally consistent in terms of cloud–radiation anomalies (i.e., low cloud leads to high OLR), while differences among the various reanalyses can be substantial (Newman et al. 2000). The precipitation in several continental regions is underestimated compared to GPCP, especially South America.

Figure 4 shows the consistency of spatial variability and ultimately the skill of several global reanalyses to reproduce the annual mean distribution of precipitation relative to GPCP in Taylor diagrams (Taylor 2001; Bosilovich et al. 2008). On these charts, CMAP provides a secondary reference and sense of the observational uncertainty. Distance from the 1, 1 point represents skill relative to the reference dataset (GPCP in this comparison). In the global comparison, MERRA and ERA-Interim are the closest to GPCP and CMAP but both also tend to be more clustered together (smaller interannual variations of the statistics). CFSR also stands out ahead of the former generation, though the variance tends to be the highest of the current generation of reanalyses. The global quality in MERRA and ERA-Interim can be attributed to the improvements over ocean regions, especially the tropical oceans. Figure 5 shows the time series of the correlation and standard deviation values used to produce the Taylor diagram for the globe and tropics (15°S–15°N), as well as the mean bias between the reanalyses and GPCP. While MERRA has the lowest biases in the tropics and in the group of low bias for the globe, it has an increasing trend relative to GPCP. On the other hand, the ERA-Interim high bias in precipitation tends to decrease in time. MERRA tropical spatial correlations are higher than any older reanalysis and are comparable to ERA-Interim and CFSR. JRA shows a strong change in precipitation correlation as SSM/I data becomes increasingly available (see also Onogi et al. 2005). The MERRA standard deviation indicates that the variance across the tropics is comparable to GPCP (which can also be said for NCEP reanalysis 1 and ERA-Interim). The representation of tropical precipitation in MERRA is much more comparable to GPCP than any the older reanalyses. At these large scales, the similarity in statistical comparison of MERRA and ERA-Interim with GPCP is remarkable. In the next section, we will evaluate the MERRA time series variability of the energy and water budget terms.

4. Time series

a. *Interannual variability*

Previous research has shown that low frequency variability in some reanalyses terms can be problematic and

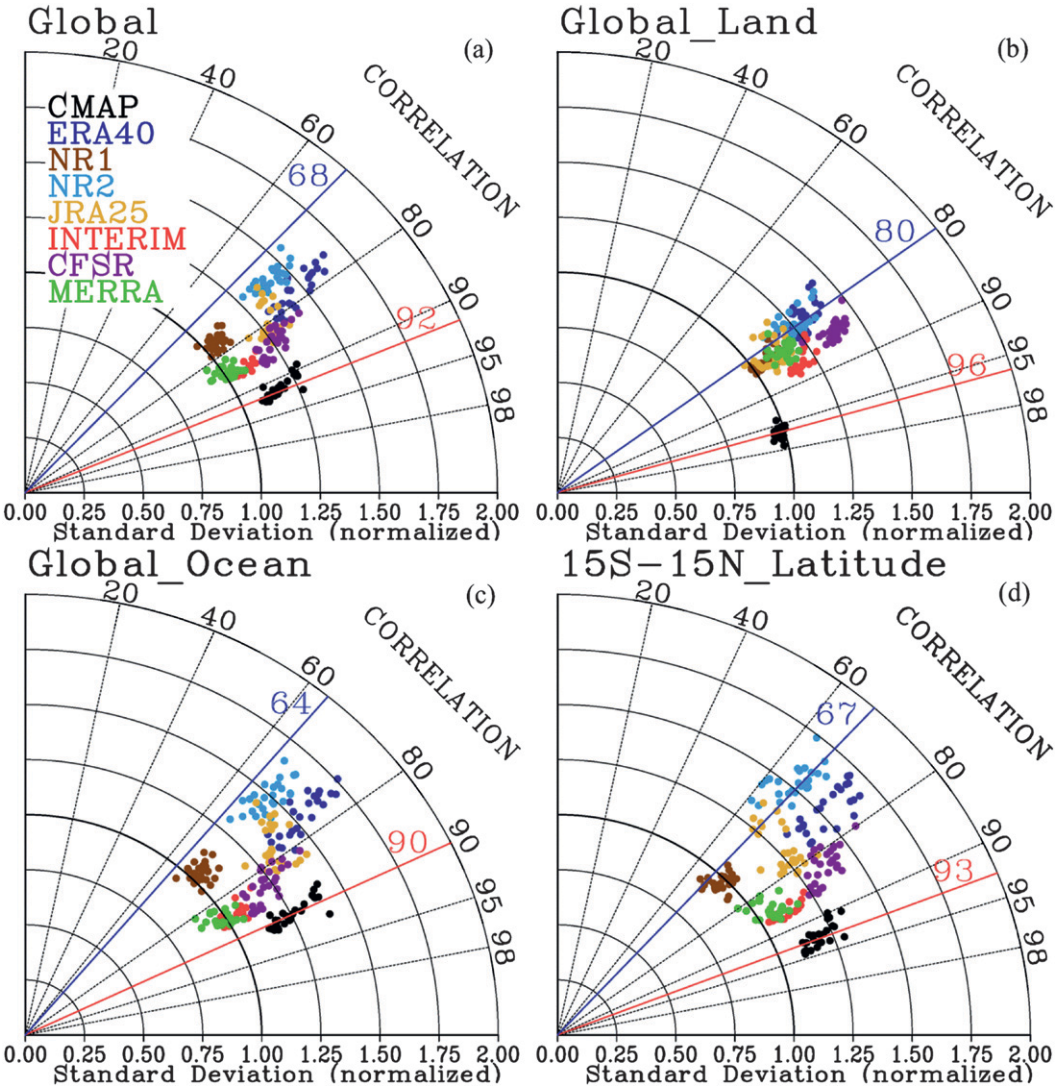

FIG. 4. Taylor diagrams of annual mean precipitation from reanalyses using GPCP as a reference and CMAP as an additional observing reference the regional statistics for the (a) globe, (b) land, (c) ocean, and (d) tropics. The red and blue lines show limits of expected high and low correlation as determined by comparing GPCP and CMAP observations. See Bosilovich et al. (2008) for details.

should be considered very carefully. While some fields in certain regions may be useful indicators of trends (Kalnay and Cai 2003), there are numerous examples of artifacts dominating real physical trends from reanalysis data. For example, ERA-40 precipitation has strong decadal interannual variability of tropical precipitation that does not appear in observations (Uppala et al. 2005; Andersson et al. 2005). Likewise, JRA-25 precipitation exhibits a stepwise shift when SSM/I retrieved total column water becomes available for assimilation (Onogi et al. 2005). In this section, we evaluate the full time series of MERRA as an extension to the 5-yr global climatological averages of the energy budget (in the previous section) and characterize the system as it changes in time.

The increasing trend in MERRA precipitation bias noted in Fig. 5 is separated into global, land, and ocean components in Fig. 6a. Precipitation over continental regions shows some periods of increase, but the global precipitation time series trends correlate more to the precipitation over ocean. The 1979–98 trend of global precipitation is +0.1 mm day^{-1} decade^{-1} (significant with $p < 0.01$), which is somewhat greater than that of GPCP (Gu et al. 2007). However, the oceanic time series beyond 1999 is not linear and undergoes a strong transition period in the late 1990s. Globally and annually integrating

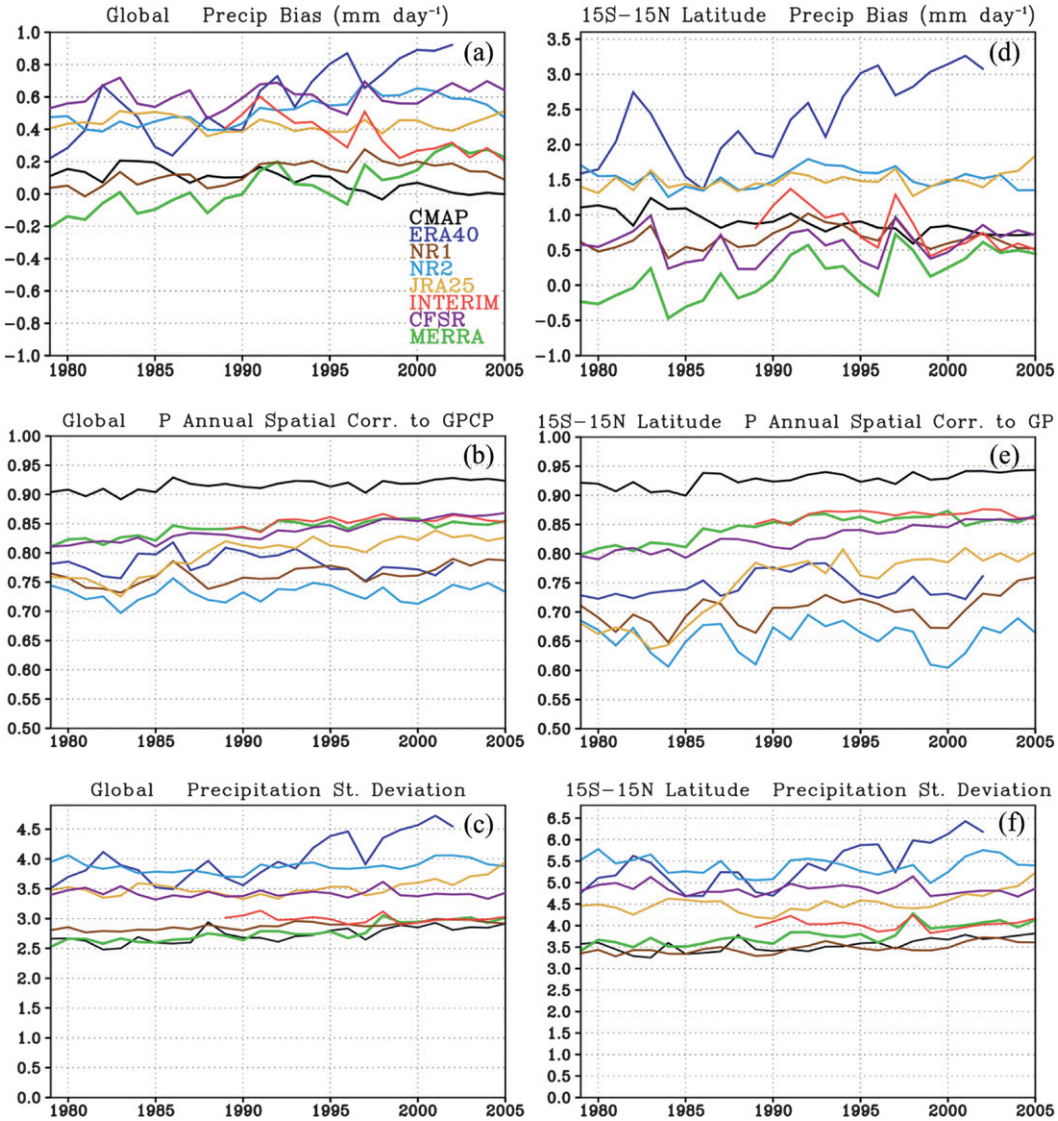

FIG. 5. Time series of annual mean statistics used in the (a)–(c) global and (d)–(f) tropics Taylor diagrams (Fig. 4a,d) for top panels mean difference form GPCP, (middle) spatial correlation to GPCP, and (bottom) standard deviation (here the black line is GPCP standard deviation, while the Taylor diagrams are normalized to GPCP standard deviation). Averages consider only grid points where valid CMAP observation only data exists.

the water budget [Eq. (3)], the precipitation is balanced both by evaporation and the analysis increment of water vapor. Some time variations apparent in global precipitation have similarities in both evaporation and, especially, the analysis increment (Fig. 6b). For example, through the early portion of the time series, evaporation is steadily increasing and exceeds precipitation by roughly 0.1 mm day^{-1} while the moisture increment is negative by a roughly similar amount. However, 1999 and 2001 each show stepwise changes in the analysis increments, which are generally reflected in the precipitation. Evaporation also responds to this change by decreasing in 1999 but responds only very weakly in 2001. After 1999, the increments act as a moisture source when the new AMSU instruments on *NOAA-15* (November 1998) and *NOAA-16* (January 2001) become available. Robertson et al. (2011) discuss the role of the AMSU-A window channels on water vapor and the possible bias correction uncertainties as the basis for the change in the water vapor increment. Precipitation is clearly sensitive to the changing observing system since the moisture increment changes propagate through the GEOS-5 moisture and radiative physics.

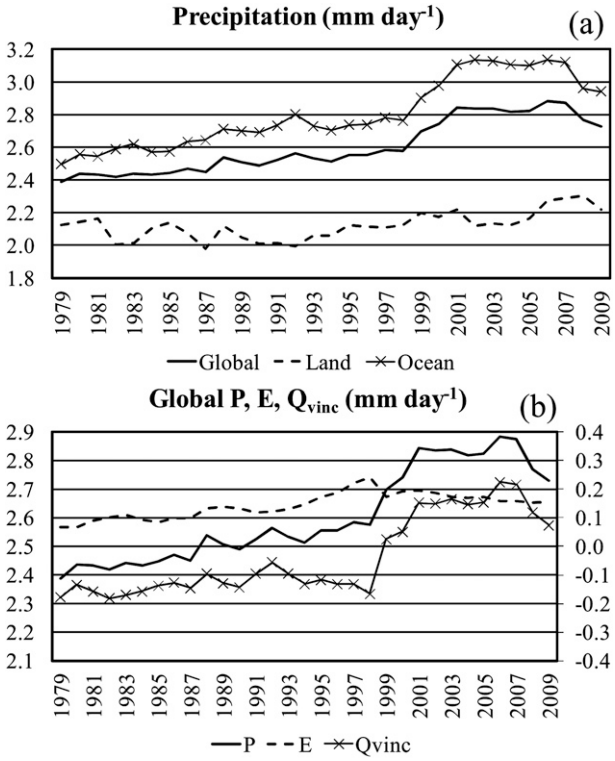

FIG. 6. Global annual averages of (a) precipitation including land-only and ocean-only averages and (b) the global annual averages of the water budget including precipitation (P), evaporation (E), and analysis increment of water vapor (Q_{vinc}).

Figure 7 examines the extent of the effect of the satellite instrument changes on the oceanic surface energy budget. The downwelling shortwave radiation (Fig. 7) follows the variations of water vapor increments (Fig. 6b) more closely than the other terms. In general, the surface shortwave radiation decreases in time while the downward surface longwave radiation increases, reflecting the increasing water vapor and clouds (not shown). The net heating of the ocean surface decreases substantially over the period with the smallest net heating bias occurring during the most modern part of the satellite era (the lowest point occurs in 2001 after which it increases steadily, Fig. 7). The downward trend in net flux to the ocean surface is almost 10 W m^{-2} over the 30-yr period and, if not accounted for, could cause significant problems if used for ocean model forcing. While downwelling shortwave radiation shows a distinct series of changes much like the water vapor increments or precipitation, the net ocean flux varies more slowly without the sharp transitions, owing to the combined influences of the surface fluxes.

Figure 8 separates the net radiative flux contributions by LW and SW components at the surface and top of the atmosphere. The surface net shortwave radiation variations exhibit the jumps in the times series, much like the analysis increments, with the surface longwave radiation changing in the opposite direction and with smaller amplitude. Likewise, the TOA net shortwave radiation has much the same variability as surface; both change from positive to negative when AMSU is being assimilated (Fig. 8) as cloud effects accompanying precipitation increases reflection. In the global average, model-simulated precipitation heating would be nearly balanced between the net radiative flux divergence between the TOA and surface. However, for the reanalysis in the presence of data assimilation, the heating increments must also be considered. Figure 9 shows the analysis increment of heat in the atmosphere (dH_{ANA}/dt). This forcing in the global energy budget is ~18 W m^{-2} in the early part of the period when satellite observations are less abundant. After 1998 the heating increments are much lower,

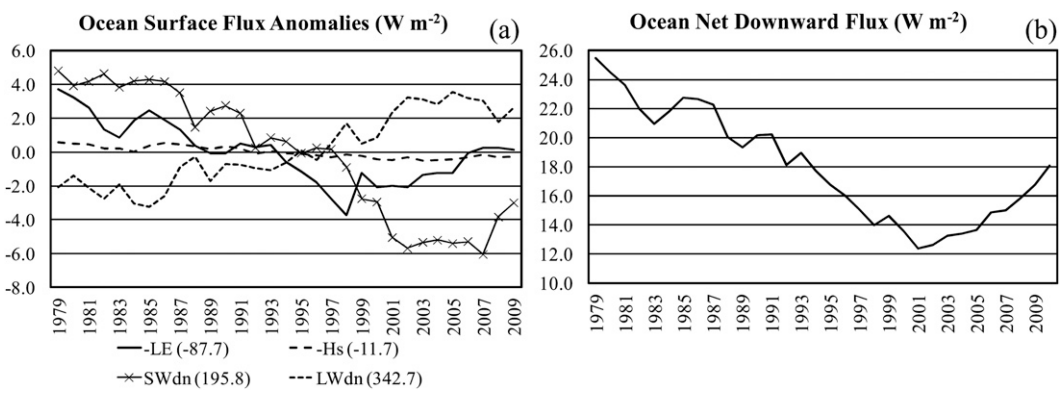

FIG. 7. Global ocean-only (a) annual anomalies for surface energy budget terms, latent heat flux (−LE), sensible heat flux (−Hs), downward shortwave radiation (SW_{dn}), and downward longwave radiation (LW_{dn}), and (b) annual mean net downward flux at the ocean surface. The mean values of the terms are oriented positive down to the surface. Mean values of the anomalies are included in the legend. Units are W m^{-2}.

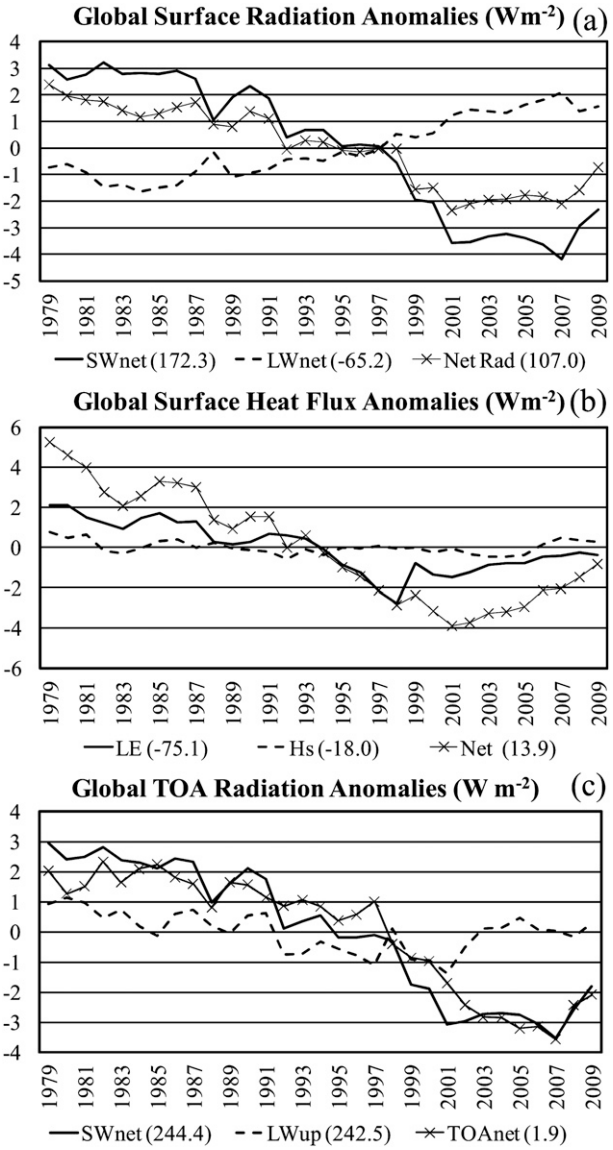

FIG. 8. Global annual anomalies for (a) net radiation terms at the surface, shortwave (SW_{net}), longwave (LW_{net}) and the net radiation, (b) surface heat fluxes (positive down) including the net heating, and (c) radiation terms at the TOA net shortwave radiation (SW_{net}), upward longwave (LW_{up}), and net top of atmosphere radiation (TOA_{net}). The means for each term are included in the legends. Units are in W m^{-2}.

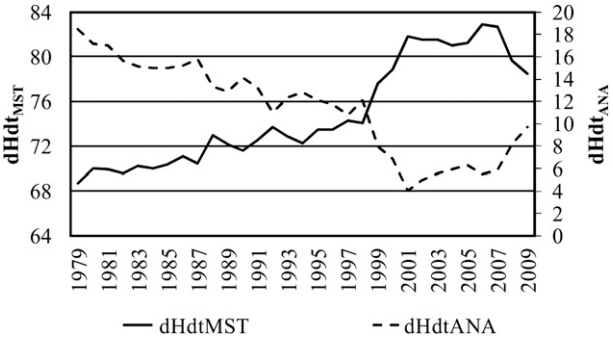

FIG. 9. Energy terms for the moist processes (MST, essentially latent heating due to precipitation) and the heating due to analysis increments. Units in W m^{-2}.

~6 W m^{-2}, but clearly sensitive to the availability of AMSU. The other striking point of Fig. 9 is the strong negative correlation between the heating increment and the vertically integrated latent heating (and so the precipitation) in the atmosphere. Figure 6b shows the water vapor increments (mm day^{-1}) alongside precipitation and evaporation global annual averages. This indicates a strong relationship between the global mean heating increments (Fig. 9), water vapor increments, and precipitation. The magnitude of the response to AMSU in atmospheric latent heating and heating increment is ~8 W m^{-2} (Fig. 9), while the net radiation (surface or TOA) is ~2–3 W m^{-2} (Fig. 8).

Figure 6 indicates that the direct effects of the new observations are more consistently present over the oceans. Given the significant extent of the observing system impact on oceanic radiative and water fluxes, we also computed the time variation of the transport of water and energy between the ocean and continental areas. Figures 10a and 10b show the anomalies of water budget terms for ocean and continental areas, including the moisture transport between them. The shift of the oceanic water vapor increments is comparable to that of the precipitation. The oceanic water vapor transport becomes more negative after 1999, indicating more water vapor leaving the oceanic areas; however, the magnitude of that change is much less than that of the water vapor increments. On the other hand, for the continental water budgets the variations in precipitation are much more closely related to the water vapor transport than the increments (Fig. 10b). The latter is the negative of the ocean transport scaled by land fraction. Trenberth et al. (2011) compare MERRA and ERA-Interim continental water vapor transports and find close correspondence between their time series. The heating of the atmosphere due to the additional water analysis increment is a substantial term in the oceanic area of the atmospheric heat budget (Fig. 10c). However, the variability of the water term is nearly opposite of the heating analysis increment so that, when the moisture increment increases dramatically in 1999, the heating increment decreases. Here, the heat transport is the sum of all heat transports, including enthalpy, kinetic energy, and latent. Then, in this area integration the total transport of heat in Figs. 10c and 10d does not show a transition in 1999, nor do any of the component energy transports (not shown). This is also evident in the continental energy budget in which the

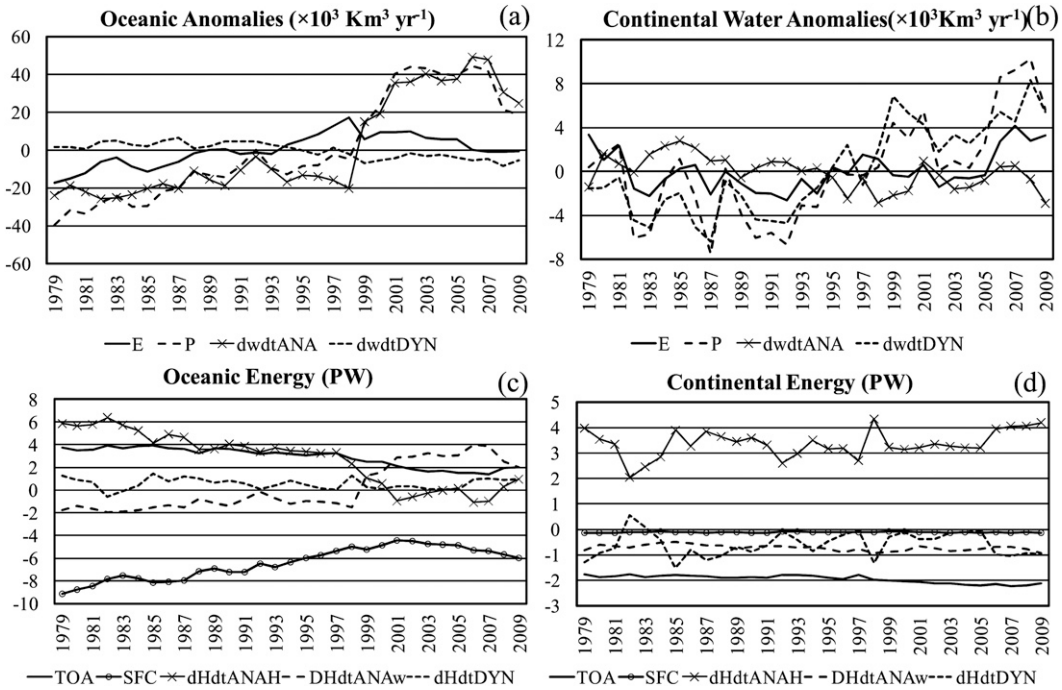

FIG. 10. Separate terms for the integrated water mass and energy budgets over land and ocean and transport: (a) ocean water budget anomalies, (b) continental budget (see Table 3 for the time means and variable definitions), (c) oceanic energy terms, and (d) land energy terms.

increments themselves do not change drastically, but rather, are fairly steady with interannual variability anticorrelated to the total heat transport (Fig. 10d). For the whole 30-yr period, then, the land energy budget values are close to those given in Table 1. In contrast to TFK09, these results indicate a weak export of energy from land to ocean and a persistent net TOA loss. This loss must be offset by the heating increment to maintain agreement in temperature and moisture with observations. From a global perspective, this underscores the fact that the effect of the transition to ATOVS is primarily over the ocean, with intermittent changes over land occurring though transport processes.

b. Spatial patterns of satellite instrument change

The previous section shows that, in the global average sense, water vapor and heating increments change noticeably with the availability of new radiance data (Fig. 6b and Fig. 10a). The onset of AMSU data availability demarcates distinct climate regimes from an energy and water balance point of view. This is especially apparent in the water budget where the globally averaged water vapor analysis increment changes sign. However, this does not provide more specific information about what regions are affected by the change.

To get a sense of the large-scale effect of this change in the observing system, we compare short time averages from before and after the start of AMSU. Decadal time averages from before AMSU (1990–97) are subtracted from time averages after (2000–08). This may include some real variations in the observed record, but the previous analysis suggests that the analysis increment change (observation system) is the globally dominant factor. Figure 11 shows the change of the water budget component tendencies and fluxes. Precipitation increases in many places, especially in the Southern Hemisphere midlatitudes and also in the tropics and South Pacific convergence zone (SPCZ). The increases in precipitation generally correspond to the locations of changes in the analysis increments, for example, in the Southern Hemisphere midlatitudes. However, the SPCZ analysis increments are smaller than the change in SPCZ precipitation but an increase in moisture convergence occurs there. It appears that the large-scale circulation has also changed significantly, as there is less convergence (more divergence) in the eastern tropical pacific. The changes in evaporation are smaller than the other terms (note the different contour levels), likely owing to the constraints of prescribed sea surface temperature and assimilated near surface wind observations. However, the evaporation decreases in the Southern Hemisphere midlatitudes where the increased moisture increments have likely decreased the near-surface humidity deficit in the bulk aerodynamic evaporation term. The increased

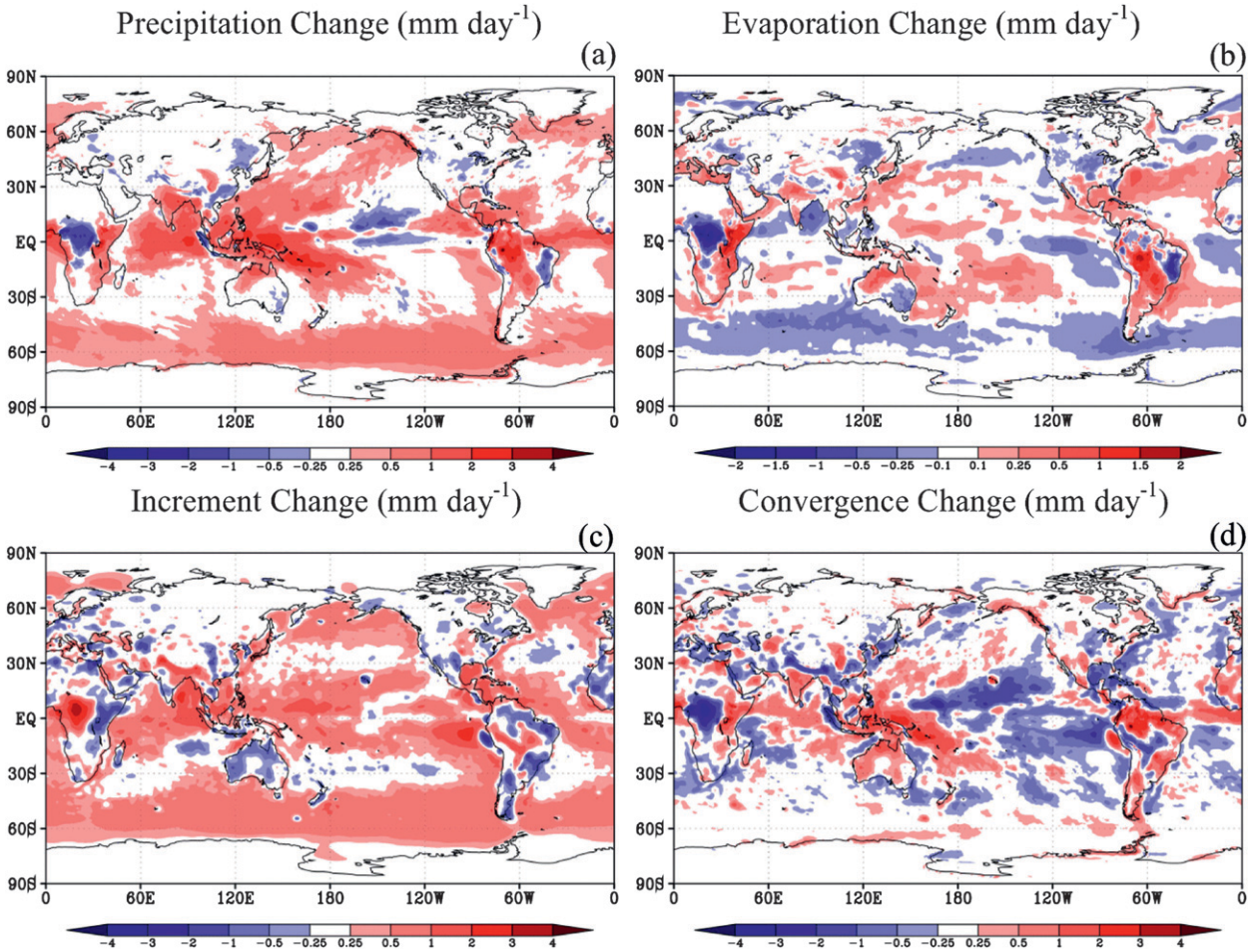

FIG. 11. Change (2000–08 minus 1990–97, after AMSU minus before) of the atmospheric hydrology budget terms: (a) precipitation, (b) evaporation, (c) incremental analysis update for water vapor, and (d) moisture convergence. The change of evaporation is smaller than other terms and is scaled different from other terms.

atmospheric water vapor has increased the cloudiness, reducing shortwave radiation (increasing longwave radiation) at the surface.

Figure 12 shows the effect of the AMSU instrument change on the atmospheric dry static energy budget terms. TOA net (downward) radiation is consistently lower in the presence of AMSU, driven less by OLR than by increasing reflected shortwave radiation due to increased clouds. The direct effect of heating increments on the radiation components is systematic with TOA net decreases over persistently cloudy eastern ocean basins, high-latitude storm tracks, and much of Africa. The changes in the analysis increments of heat are quite variable over continental regions, but they appear to be balanced solely by the vertically integrated heat convergence and release of total potential energy. At the surface energy losses dominate over ocean regions, except in the Southern Ocean where downward heat flux increases with decreased latent heat flux. However, the atmosphere also reacts by redistributing the energy dynamically by transport (note the difference in contour intervals in each panel), consistent with the time series data presented in Fig. 10. This may also hold over the oceanic basins as well, except that there is imbalance of energy due to prescribed SSTs, whereas the land model balances energy over the continental surfaces. The effect of the AMSU generally reaches all of the water and energy components over oceans, especially the warm pool and Southern Hemisphere midlatitudes, so these regions will have features related to the changing observing system in the long time series. In a companion effort, Robertson et al. (2011) diagnose these satellite sensor effects in more detail.

In the analysis presented thus far, a widespread systematic change with time of the water cycle components (Fig. 11) appears over the oceans, but with more subtle

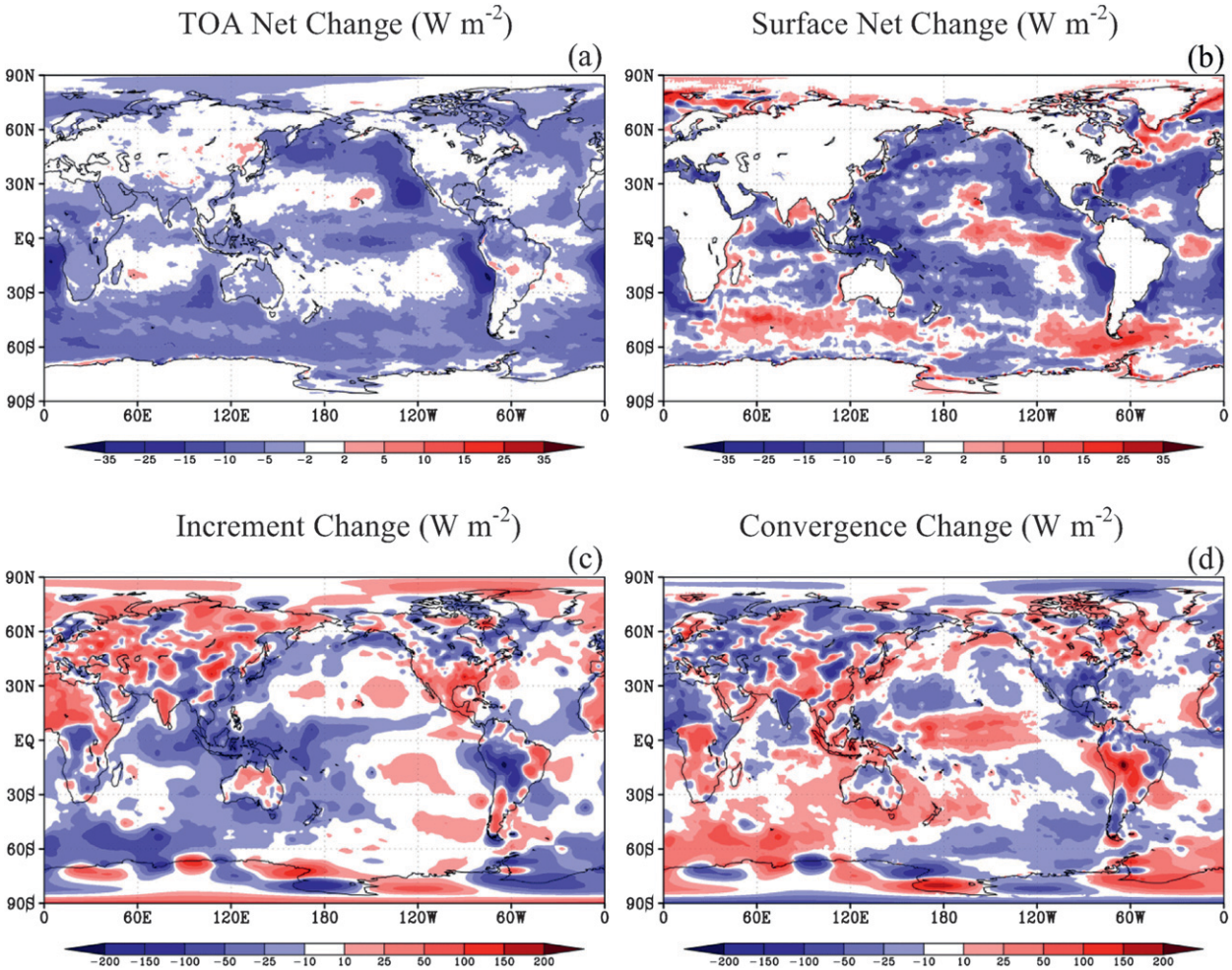

FIG. 12. Change (2000–08 minus 1990–97, after AMSU minus before) of the atmospheric energy budget terms: (a) net TOA radiation, (b) net surface energy flux, (c) incremental analysis update for dry static heat, and heat convergence.

apparent effects over the continents. However, the tropical continental regions do show some variations; here we consider the anomalies in the Amazon River basin and central Africa. Figure 13 shows the time series of root-zone soil water for the Amazon River basin (the area is similar to that used in Bosilovich and Chern 2006, their Fig. 1). In conjunction with the start of AMSU instrumentation, the soil water becomes systematically higher than in previous years, which agrees with the increase in precipitation noted in Fig. 11a. Figure 14 compares the mean annual cycle of precipitation in the Amazon Basin before and after the start of AMSU for both GPCP merged gauge–satellite rain rate and that of MERRA. MERRA appears to have a low bias before AMSU, mostly focused on the transition from the dry to wet season. But after AMSU, MERRA produces more precipitation than the observed data. The AMSU period (1999–2006) has shifted phase compared to the earlier period, and also compared to observations. It interesting to note that GPCP wet season precipitation in the later period is higher than the earlier period, which may indicate a real increase in the region. Nonetheless, the change in the Amazon is concomitant with the changing observing systems and its effect reaching the large tropical river basin. Given that evaporation, moisture convergence, and the water vapor increments are also changing in time (Fig. 11), a more thorough analysis of this region, beyond the scope of the present study, is planned.

In central Africa a significant hydrologic anomaly occurs, and its sign contrasts with the general changes over the oceans and also over the Amazon River basin. In time, precipitation and evaporation are decreasing while the area becomes more divergent despite increasing vertically integrated water vapor increments. Figure 15a shows the comparison of MERRA precipitation with

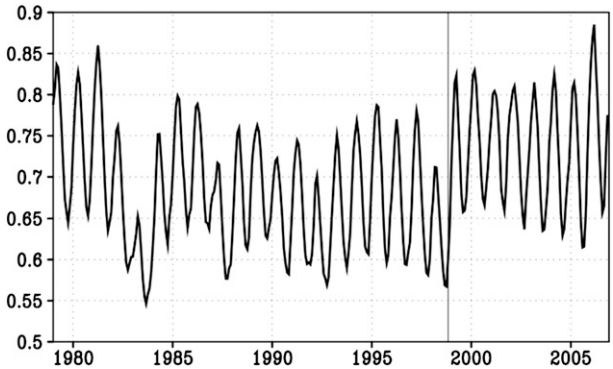

FIG. 13. Time series of MERRA monthly mean root zone soil wetness fraction (nondimensional), area averaged over the Amazon River basin.

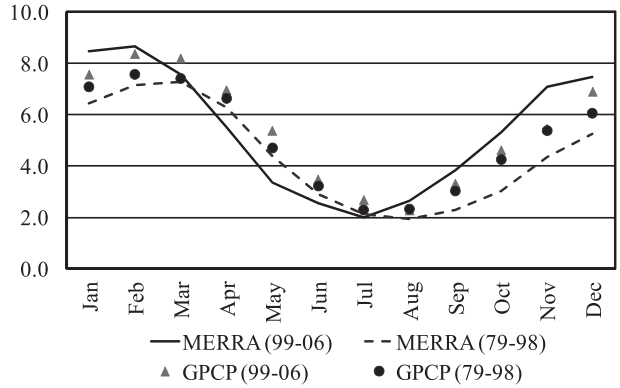

FIG. 14. Mean annual cycle of monthly precipitation (mm day^{-1}) area-averaged over the Amazon River basin from MERRA before AMSU data (1979–98, dashed line) and MERAA when AMSU data is assimilated (1999–2006), solid line, and also the corresponding GPCP (Adler et al. 2003) basin-averaged precipitation (● for 1979–98, ▲ for 1999–2006).

that of a station near the center of the low anomaly. MERRA precipitation is fairly comparable to the local observations early in the reanalysis, but exhibits a sharp drop of local precipitation in late 1995. Over the region the area becomes warm and dry, with precipitation less than observed.

Further investigation of the MERRA assimilated observations shows that a single radiosonde station (Bangui, Station ID 64650) is present in the interior of the continent near the anomaly, while additional stations are only available at the coasts during most of the period. Figure 15b shows the monthly mean time series of 850-mb specific humidity anomalies from Bangui, compared with MERRA monthly water vapor anomalies (grid point at 4.5°N, 18.667°E). The radiosonde station water vapor drops substantially in time with MERRA precipitation, but we also see that MERRA water vapor analysis tracks the observations. Since this is the only nearby radiosonde and satellite data are not as prevalent over land, this station's observations influence the area radiating out for several hundred kilometers. In time, the surface becomes dry and warm following the unusually persistent low precipitation. Eventually the atmospheric circulation is affected and subsidence forms over the region, possibly related to the AMSU observations—even further limiting the extent of the precipitation. The feature also appears in operational analyses surface flux field comparisons with remotely sensed merged flux data (Vinukollo et al. 2011). Preliminary investigation in the documentation of this station indicates that the ground station equipment was changed in the mid-1990s (L. Haimberger 2010, personal communication). These results emphasize the continuing need for consideration of the input observations and even metadata to best interpret the reanalysis results (Dee et al. 2011).

5. Summary and conclusions

The MERRA representation of the earth's water and energy cycle climatology has several advantages over existing reanalyses but also weaknesses that have affected past reanalyses as well. The MERRA climatological precipitation field has a small global mean bias and improved spatial correlation compared to the existing global reanalyses, especially across the tropics, and is

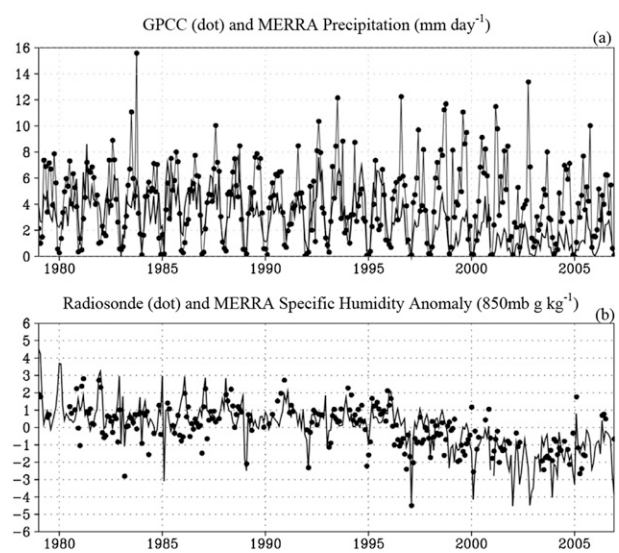

FIG. 15. Time series of monthly MERRA data compared to observations at the MERRA point (4.5°N, 18.67°E): (a) GPCC precipitation (dots with thin line; Schneider et al. 2008) and MERRA precipitation (thick solid line) and (b) Bangui radiosonde observations (dots, station ID 64650, 4.24°N, 18.31°E) of 850-mb specific humidity anomaly compared to MERRA. The anomalies were calculated by removing the mean annual cycle.

also very similar to the ECMWF Interim reanalyses in that regard. The MERRA spatial resolution is finer than many of the previous generation reanalyses and the number of variables produced is extensive. An important feature is that the system budget equations are represented entirely and can be closed. This closure requires the analysis increment term, representing the part of the model budgets that ensures the state variable ''trajectory'' in the reanalysis stays as close as possible to observations. The analysis increments play a crucial role in the present evaluation of the global water and energy cycles, embodying the influences of observations as well as the biases in model physics. Characterization of the strengths and weaknesses requires consideration not only of the model physical processes but, as emphasized here, the nature of the evolving observational record.

Comparing the MERRA global climate energy budgets with previous studies and observations (e.g., TFK09), some consistent biases become apparent. Cloud effects and many of the surface and TOA radiation components suggest that MERRA clouds are optically weaker than reality (too few or too thin). This allows excessive shortwave radiation at the surface, especially over oceans. Time series analysis shows a decreasing trend in the shortwave radiation at the surface, which is a general improvement to the surface energy balance. However, the time series also shows that major stepwise changes occur in MERRA, most notably in the oceanic precipitation. These changes are clearly tied to the analysis increment and are concurrent with the addition of new satellite instrumentation. This is not a new feature in reanalyses, as the JRA-25 has a clear dependency on the availability of SSM/I, and CFSR and ERA-Interim reanalyses also show precipitation variation around the time of *NOAA-15* and *NOAA-16*. Nonetheless, this identifies a general limitation and challenge that must be addressed in future reanalyses (Thorne and Vose 2010 and Dee et al. 2011).

The strongest shifts in the MERRA water and energy budgets coincide with the availability of AMSU instruments in 1999 and 2001. A concurrent study (Robertson et al. 2011) uses principal component analysis to quantify and remove the observing system variations from some of the physical terms time series. In addition, this work shows strong evidence that the sensitivity of the reanalysis is related to AMSU-A window channels. Here, we have assessed the broad impact on the water and energy budgets. The direct effect is largely related to oceanic regions (especially the Southern Hemisphere midlatitudes and tropical western Pacific and Indian Oceans), though dynamical transports are significant in linking forcing over ocean to processes over land, but the effect is more pronounced in some regions than others. The new data lead to more precipitation, total column water, and clouds, with less net radiation at the surface and less net radiation leaving at the top of the atmosphere.

The changes in the state of the water balance over the ocean differ in important ways from those over the land. The transport between land and ocean does not correlate with the analysis increments over land. Rather, precipitation over land is linked most closely to transport from the ocean. This suggests that satellite epoch changes (e.g., AMSU-A availability) do indirectly affect the MERRA water and energy balance over land through altered moisture and heat transport, as indicated by variations over the Amazon River basin. Even so, the dominant data type over land, radiosondes, can strongly influence MERRA state variables, physics quantities, and the trends. This can be demonstrated in central Africa where a single station influences a large region's water and energy cycles. The observational inputs to reanalyses are quite sizable and have improved demonstrably over the years. These iterations are clarifying the uncertainties that still exist, as well as their origin in both model physics and in the quality of the input data stream. It is important for individual researchers to be aware of variations in the observing system in regards to the science objectives of their research, and independent verification and even intercomparisons of reanalyses is needed. MERRA provides the analysis increments that can be used by researchers to better understand the observations and analyses (as suggested by Dee et al. 2011). Furthermore, assimilated observations will also be made available (as demonstrated in the African sonde comparisons). Newer observing systems and different observations (e.g., soil moisture, clouds or aerosols) may have even larger impact if there is no long record of the data or multiple overlapping instruments. Addressing variations of the observing system in the reanalysis data assimilation is a priority for continuing research, development, and production of reanalyses.

Acknowledgments. MERRA was developed with support from the NASA Modeling, Analysis and Prediction program. This study was supported by the NASA Energy and Water cycles Studies (NEWS) program. The work also benefitted from thoughtful comments from the NEWS Modeling working group and the NEWS Global Energy Climatology working group. Siegfried Schubert, Kevin Trenberth, and Paul Stackhouse also provided many thoughtful suggestions over the course of this study. Russell Vose and Leopold Haimberger provided valuable insights and discussions about the Bangui station. We appreciate the useful comments and thoughtful review by four anonymous reviewers.

REFERENCES

Adler, R. F., and Coauthors, 2003: The version-2 Global Precipitation Climatology Project (GPCP) monthly precipitation analysis (1979–present). *J. Hydrometeor.,* **4,** 1147–1167.

Andersson, E., and Coauthors, 2005: Assimilation and modeling of the atmospheric hydrological cycle in the ECMWF forecasting system. *Bull. Amer. Meteor. Soc.,* **86,** 387–402.

Bengtsson, L., and J. Shukla, 1988: Integration of space and in situ observations to study global climate change. *Bull. Amer. Meteor. Soc.,* **69,** 1130–1143.

——, S. Hagemann, and K. I. Hodges, 2004: Can climate trends be calculated from reanalysis data? *J. Geophys. Res.,* **109,** D11111, doi:10.1029/2004JD004536.

Bloom, S. C., L. L. Takacs, A. M. da Silva, and D. Ledvina, 1996: Data assimilation using incremental analysis updates. *Mon. Wea. Rev.,* **124,** 1256–1271.

Bosilovich, M. G., and S. D. Schubert, 2001: Precipitation recycling over the central United States diagnosed from the GEOS-1 data assimilation system. *J. Hydrometeor.,* **2,** 26–35.

——, and J.-D. Chern, 2006: Simulation of water sources and recycling for The MacKenzie, Mississippi, and Amazon River basins. *J. Hydrometeor.,* **7,** 312–329.

——, J. Chen, F. R. Robertson, and R. F. Adler, 2008: Evaluation of global precipitation in reanalyses. *J. Appl. Meteor. Climatol.,* **47,** 2279–2299.

——, D. Mocko, J. O. Roads, and A. Ruane, 2009: A multimodel analysis for the Coordinated Enhanced Observing Period (CEOP). *J. Hydrometeor.,* **10,** 912–934.

Chen, J., A. D. Del Genio, B. E. Carlson, and M. G. Bosilovich, 2008a: The spatiotemporal structure of twentieth-century climate variations in observations and reanalyses. Part I: Long-term trend. *J. Climate,* **21,** 2611–2633.

——, ——, ——, and ——, 2008b: The spatiotemporal structure of twentieth-century climate variations in observations and reanalyses. Part II: Pacific pan-decadal variability. *J. Climate,* **21,** 2634–2650.

Cullather, R. I., and M. G. Bosilovich, 2011a: The moisture budget of the polar atmosphere in MERRA. *J. Climate,* **24,** 2861–2879.

——, and ——, 2011b: The energy budget of the polar atmosphere in MERRA. *J. Climate,* in press.

Dee, D. P., E. Källén, A. J. Simmons, and L. Haimberger, 2011: Comments on ''Reanalyses suitable for characterizing long-term trends.'' *Bull. Amer. Meteor. Soc.,* **92,** 65–70.

Fasullo, J. T., and K. E. Trenberth, 2008a: The annual cycle of the energy budget. Part I: Global mean and land–ocean exchanges. *J. Climate,* **21,** 2297–2312.

——, and ——, 2008b: The annual cycle of the energy budget. Part II: Meridional structures and poleward transports. *J. Climate,* **21,** 2313–2325.

GMAO, cited 2011: The MERRA atlas. [Available online at http://gmao.gsfc.nasa.gov/ref/merra/atlas/.]

Gu, G., R. F. Adler, G. J. Huffman, and S. Curtis, 2007: Tropical rainfall variability on interannual-to-decadal and longer time scales derived from the GPCP monthly product. *J. Climate,* **20,** 4033–4046.

Kalnay, E., and M. Cai, 2003: Impact of urbanization and land-use change on climate. *Nature,* **423,** 528–531.

——, and Coauthors, 1996: The NCEP/NCAR 40-Year Reanalysis Project. *Bull. Amer. Meteor. Soc.,* **77,** 437–471.

Kanamitsu, M., W. Ebisuzaki, J. Woollen, S.-K. Yang, J. J. Hnilo, M. Fiorino, and G. L. Potter, 2002: NCEP-DOE AMIP-II Reanalysis (R-2). *Bull. Amer. Meteor. Soc.,* **83,** 1631–1643.

Loeb, N. G., B. A. Wielicki, D. R. Doelling, G. L. Smith, D. F. Keyes, S. Kato, N. Manalo-Smith, and T. Wong, 2009: Toward optimal closure of the earth's top-of-atmosphere radiation budget. *J. Climate,* **22,** 748–766.

Maurer, E. P., G. M. O'Donnell, and D. P. Lettenmaier, 2001: Evaluation of the land surface water budget in NCEP/NCAR and NCEP/DOE reanalyses using an off-line hydrologic model. *J. Geophys. Res.,* **106,** 17 841–17 862.

Newman, M., P. D. Sardeshmukh, and J. W. Bergman, 2000: An assessment of the NCEP, NASA, and ECMWF reanalyses over the tropical west Pacific warm pool. *Bull. Amer. Meteor. Soc.,* **81,** 41–48.

Onogi, K., and Coauthors, 2005: JRA-25: Japanese 25-year reanalysis project—Progress and status. *Quart. J. Roy. Meteor. Soc.,* **131,** 3259–3268.

——, and Coauthors, 2007: The JRA-25 Reanalysis. *J. Meteor. Soc. Japan,* **85,** 369–432.

Rienecker, M., and Coauthors, 2007: The GEOS-5 data assimilation system—Documentation of versions 5.0.1 and 5.1.0. NASA GSFC Tech. Rep. Series on Global Modeling and Data Assimilation, NASA/TM-2007-104606, Vol. 27, 92 pp.

——, and Coauthors, 2011: MERRA: NASA's Modern-Era Retrospective Analysis for Research and Applications. *J. Climate,* **24,** 3624–3648.

Roads, J. O., and A. K. Betts, 2000: NCEP–NCAR and ECMWF reanalysis surface water and energy budgets for the Mississippi River basin. *J. Hydrometeor.,* **1,** 88–94.

——, M. Kanamitsu, and R. Stewart, 2002: CSE water and energy budgets in the NCEP–DOE reanalysis II. *J. Hydrometeor.,* **3,** 227–248.

Roberts, J. B., F. R. Robertson, C. A. Clayson, and M. G. Bosilovich, 2011: Characterization of turbulent latent and sensible heat flux exchange between the atmosphere and ocean in MERRA. *J. Climate,* in press.

Robertson, F. R., M. G. Bosilovich, J. Chen and T. L. Miller 2011: The effect of satellite observing system changes on MERRA water and energy fluxes. *J. Climate,* **24,** 5197–5217.

Saha, S., and Coauthors, 2010: The NCEP climate forecast system reanalysis. *Bull. Amer. Meteor. Soc.,* **91,** 1015–1057.

Schlosser, C. A., and P. R. Houser, 2007: Assessing a satellite-era perspective of the global water cycle. *J. Climate,* **20,** 1316–1338.

Schneider, U., T. Fuchs, A. Meyer-Christoffer, and B. Rudolf, cited 2008: Global precipitation analysis products of the GPCC. Global Precipitation Climatology Centre (GPCC), DWD Internet Publication, 1–12. [Available online at ftp://ftp-anon.dwd.de/pub/data/gpcc/PDF/GPCC_intro_products_2008.pdf.]

Schubert, S. D., and Y. Chang, 1996: An objective method for inferring sources of model error. *Mon. Wea. Rev.,* **124,** 325–340.

Simmons, A., S. Uppala, and D. Dee, 2007: Update on ERA-Interim. *ECMWF Newsletter,* No. 111, ECMWF, Reading, United Kingdom, 5. [Available online at http://www.ecmwf.int/publications/newsletters/pdf/111.pdf.]

Suarez, M., and Coauthors, cited 2011: File specification for MERRA products. Global Modeling and Assimilation Office. [Available online at http://gmao.gsfc.nasa.gov/research/merra/file_specifications.php.]

Taylor, K. E., 2001: Summarizing multiple aspects of model performance in a single diagram. *J. Geophys. Res.,* **106** (D7), 7183–7192.

Thorne, P. W., and R. S. Vose, 2010: Reanalyses suitable for characterizing long-term trends. *Bull. Amer. Meteor. Soc.,* **91,** 353–361.

Trenberth, K. E., and J. G. Olson, 1988: An evaluation and intercomparison of global analyses from the National

Meteorological Center and the European Centre for Medium Range Weather Forecasts. *Bull. Amer. Meteor. Soc.,* **69,** 1047–1057.

——, L. Smith, T. Qian, A. Dai, and J. Fasullo, 2007: Estimates of the global water budget and its annual cycle using observational and model data. *J. Hydrometeor.,* **8,** 758–769.

——, J. T. Fasullo, and J. Kiehl, 2009: Earth's global energy budget. *Bull. Amer. Meteor. Soc.,* **90,** 311–323.

——, ——, and J. Mackaro, 2011: Atmospheric moisture transports from ocean to land and global energy flows in reanalyses. *J. Climate,* **24,** 4907–4924.

Uppala, S. M., and Coauthors, 2005: The ERA-40 Re-Analysis. *Quart. J. Roy. Meteor. Soc.,* **131,** 2961–3012.

——, D. Dee, S. Kobayashi, P. Berrisford, and A. Simmons, 2008: Towards a climate data assimilation system: Status update of ERA-Interim. *ECMWF Newsletter,* No. 115, ECMWF, Reading, United Kingdom, 12–18. [Available online at http://www.ecmwf.int/publications/newsletters/pdf/115.pdf.]

Vinukollu, R., J. Sheffield, E. F. Wood, M. G. Bosilovich, and D. Mocko, 2011: Multimodel analysis of energy and water fluxes: Intercomparisons between operational analyses, a land surface model, and remote sensing. *J. Hydrometeor.,* in press.

Wu, W.-S., R. J. Purser, and D. F. Parrish, 2002: Three-dimensional variational analysis with spatially inhomogeneous covariances. *Mon. Wea. Rev.,* **130,** 2905–2916.

Xie, P., and P. A. Arkin, 1996: Global precipitation: A 17-year monthly analysis based on gauge observations, satellite estimates, and numerical model outputs. *Bull. Amer. Meteor. Soc.,* **78,** 2539–2558.

Yu, L., and R. A. Weller, 2007: Objectively analyzed air–sea heat fluxes for the global ice-free oceans (1981–2005). *Bull. Amer. Meteor. Soc.,* **88,** 527–539.